European Polymer Journal 223 (2025) 113629

Contents lists available at ScienceDirect

European Polymer Journal

journal homepage: www.elsevier.com/locate/europolj

Highly pure curing agent from tomato waste for bio-based anti-corrosion epoxy coatings

Raffaella Suriano [a,*], Mirko Magni [b,*], Beatrice Tagliabue [a], Valentina Re [a], Riccardo Ciapponi [a], Rita Nasti [b], Marco Cavallaro [a], Giangiacomo Beretta [b], Stefano Turri [a], Marinella Levi [a]

[a] Department of Chemistry, Materials and Chemical Engineering "Giulio Natta", Politecnico di Milano, Piazza Leonardo da Vinci 32, 20133 Milano, Italy
[b] Department of Environmental Science and Policy, Università Degli Studi di Milano, Via Celoria 2, 20133 Milano, Italy

ARTICLE INFO

Keywords:
Metal protection coatings
bisphenol A-free
Agri-food waste
Glass transition temperature
Electrochemistry
Accelerated aging test

ABSTRACT

Tomato peels have been proposed as a promising biowaste for producing bio-derived anti-corrosion polymer coatings potentially more sustainable than traditional petrol-based ones. Nonetheless, there is no proof that the cutin monomer, i.e. 10,16-dihydroxy hexadecanoic acid (10,16-diHHDA) largely found in tomato peel, can be used as a curing agent, due to a lack of sufficiently pure samples of this fatty acid. In this work, the cutin monomer was firstly successfully isolated by up-cycling tomato-dried peels with a purity averaging 92 % and a 67 % recovery rate. 10,16-diHHDA was then used as a trifunctional reactive component to develop fully bio-based epoxy coatings formulated with three different epoxidized precursors. Using a phloroglucinol epoxidized precursor, an increase in the ratio between epoxy groups and hydrogen-active nucleophiles increased the glass transition temperature, up to an average of 104 °C, along with enhanced hardness and adhesion to steel and aluminum alloy surfaces. Additionally, all the cutin-derived coatings exhibited higher hydrophobicity than a reference bisphenol-A-containing coating. The most promising bio-based resin formulations were finally used to coat carbon steel samples and the protection ability against corrosion in a 3.5 wt% NaCl solution was assessed through a multi-step electrochemical testing protocol to investigate continuum phenomena at both medium|coating and coating|metal interfaces. As a result, two resin compositions (namely PC_4:1_5 and PC_5:1_3, differing for the amounts of the cutin monomer and catalyst) were identified as the most protective coatings in terms of both instant and long-term performance. Pore resistance, initially $\geq$ 100 GΩ cm^2 on average, double that of the reference petrol-based coating, decreased to a still well-satisfactory 1 GΩ cm^2 value even after one week of accelerated aging test. Within the same time frame (i.e., 7 times longer than the recommended period by the ASTM industrial standard test) the water uptake was finally set at <5 % values without any delamination.

1. Introduction

The transition from a fossil-based to a sustainable economy is crucial for reducing our society's dependence on fossil resources and decreasing environmental pollution resulting from fossil fuel consumption, which leads to greenhouse gas emissions [1]. In this contest, bioeconomy, defined as an economy using renewable biological resources from the land and sea as inputs to produce food, material, and energy [2], possesses a high potential to boost this economic transition, which can lead to circular bioeconomy if agro-industrial wastes are used to produce chemicals and fuels [3,4]. A specific example of agro-waste valorization is the conversion of tomato wastes into energy, chemicals, biocatalysts, biopolymers, bio-additives, etc. [5]. An estimated 1–2 million tons of tomato waste [6] is generated annually during fresh tomato processing, which is necessary for making products like tomato sauce and ketchup – representing over 60 % of tomato products in the EU [7]. Tomato waste is currently disposed of in uncontrolled and controlled landfills, with a negative environmental impact [8]. Instead of disposing of tomato product residues, they can be utilized for animal feeding, fertilization, and producing raw materials such as chemicals and biopolymers [9]. For example, tomato peels contain significant amounts of pectin, employed as a tin corrosion inhibitor [10], and cutin, used for producing and plasticizing bioplastics [11,12].

Cutin is a bio-polyester contained in various fruit cuticles and consists of esterified tri- and bi-functional fatty acids [13], which form an amorphous 3D network, capable of regulating water uptake/egress and

* Corresponding authors.
E-mail addresses: raffaella.suriano@polimi.it (R. Suriano), mirko.magni@unimi.it (M. Magni).

https://doi.org/10.1016/j.eurpolymj.2024.113629
Received 30 September 2024; Received in revised form 23 November 2024; Accepted 5 December 2024
Available online 10 December 2024

protecting the internal parts of fruits towards, among others, mechanical stresses and UV radiation. The function of tomato cuticles is remarkably similar to that of artificial organic coatings used to protect various human-made objects. The primary molecule in tomato cuticles is 10,16-dihydroxy hexadecanoic acid (10,16-diHHDA) [14]. This compound can be extracted by either dewaxing isolated cuticles or alkaline hydrolysis [15]. A mixture of hydroxy fatty acids derived from the cutin was employed to develop a bio-based polyester-based coating for metal protection [16], food canning [17–19], and packaging applications [20,21]. Poly(ester-urethane) coatings for cellulose-based paper substrates were recently derived from tomato peels [22].

Epoxy coatings are often used to protect metals and alloys against corrosion due to their effectiveness [23]. They dominate the organic protective coating market, despite concerns about their environmental sustainability and health impacts [24]. Most thermosetting epoxy materials are currently composed of diglycidyl ether of bisphenol A (DGEBA), which provides strong thermal resistance, mechanical performance, and good corrosion protection. However, bisphenol A (BPA) is an endocrine disruptor for living beings, because it can interact with human hormone receptors, causing harmful health effects, including alterations in brain chemistry, immune systems, and reproductive systems in various animals [25,26]. The toxicity of these materials, combined with the global tendencies toward the principles of sustainable development, has stimulated the research of renewable resources to develop bio-based epoxy building blocks [27,28], e.g. cardanol-based [29,30], vegetable oil-derived [31,32] and isosorbide-based epoxy resins [33]. To achieve the ultimate durable coating, it is crucial to combine and react epoxidized pre-polymers with curing agents, including amines (both aliphatic/aromatic and primary/secondary), phenols, carboxylic acids, thiols, and anhydrides. They are almost invariably derived from fossil sources and sometimes even toxic. To reduce their health and environmental concerns, curing agents can be derived from renewable sources such as citric acid and cashew nut shell liquid crosslinked with epoxy resins for anti-corrosion coatings [34] and superhydrophobic oil/water separation media [35]. A bio-based curing agent was also obtained from cashew nutshells cardanol to convert epoxidized soybean oil into a thermosetting epoxy coating [25,26,36].

Despite numerous bio-oriented studies, literature still lacks reporting on the performance of the highly pure 10,16-diHHDA molecule obtained from upcycling tomato waste [18,19]. Montanari *et al.* described the development of coatings obtained by curing a bio-based mixture of (poly)hydroxyl acids (derived from tomato peels) with phenolic or polyisocyanate reagents [18]. Benítez *et al.* reported the production of protective thin films by polycondensation of a mixture of bio-based lipids derived by the treatment of tomato pomace [19]. However, there is a knowledge gap in assessing the potential of the 10,16-diHHDA cutin monomer in coating formulations. For instance, it can be employed as a curing agent for bio-based epoxy resins to produce thermosetting coatings that are free of bisphenol A (BPA-free) or non-intent (BPA-NI), suitable for anti-corrosion applications. Utilizing cutin-derived monomers has the potential to introduce a dual innovation to the organic coating industry. First, it can accelerate the transition to a bio-based economy by utilizing agri-food waste as a valuable curing agent, reducing the reliance on fossil-based sources. Secondly, the 10,16-diHHDA molecule exhibits multifunctionality, possessing two hydroxyl groups and a carboxylic acid group. These unique properties enable the production of highly crosslinked polymer networks suitable for thermosetting coatings.

This work aimed to prepare a series of fully bio-based BPA-free epoxy coatings crosslinked by using highly pure 10,16-diHHDA monomer upcycled through the depolymerization of cutin contained in tomato peel waste. By screening different bio-based epoxy resins available on the market, such as epoxidized cardanol, sorbitol, and phloroglucinol, the formulation bearing phloroglucinol triglycidyl ether (PHTE) was selected for further optimization as it exhibited the best performance in terms of glass transition temperature, T_g. By changing the epoxy vs. curing agent ratio and catalyst amount, several coating compositions were tested to determine the most promising ones and guarantee high outdoor thermal resistance and good mechanical properties. Adhesion strengths, surface energies, and hardness levels on steel and aluminum alloy substrates were evaluated for the selected coating compositions. Eventually, the anticorrosion properties of the selected coatings were characterized using electrochemical impedance spectroscopy (EIS) and modified, harsher accelerated cyclic electrochemical technique (ACET) tests. Results firstly evidence the possibility of developing fully bio-based and BPA-free/BPA-NI epoxy resins for corrosion protection by employing a highly pure and stable dihydroxy acid curing agent upcycled by tomato peel waste.

2. Experimental section

2.1. Materials

The bio-based resin derived from cardanol, named NC-547 (compound **a** in Fig. 1), was kindly supplied by Cardolite Corporation and it is characterized by an equivalent epoxy weight (EEW) of 550–850 g/eq, whereas the epoxidized-sorbitol resin named EX-622 (**b**, Fig. 1) was kindly supplied by Nagase ChemteX Corporation (EEW = 189 g/eq).

Phloroglucinol Tris Epoxy (PHTE, **c** in Fig. 1) resin was purchased from Specific Polymers and the epoxy content determined by NMR titration was 8.3 meq/g. DGEBA (**d**, Fig. 1) was purchased from Merck (Milano, Italy). Two different chemicals have been used as curing agents: 10,16-diHHDA (**e**, Fig. 1), derived from the depolymerization of cutin from tomato peel waste as described in the next section, and hexahydro-4-methylphtalic anhydride (HMPA) (**f**, Fig. 1) purchased from Sigma Aldrich. 2-methylimidazole purchased from Merck (Milano, Italy) was used as the catalyst (**g**, Fig. 1). Sodium hydroxide (NaOH, granulated, purity >98.0 %) was stored under an inert atmosphere due to its hygroscopicity and purchased from Tokyo Chemical Industry Co., Ltd. Methanol (MeOH, Ph.Eur.-Reag. ACS analytical reagent) was provided by VWR Chemicals BDH. Water Milli-Q®, hydrochloric acid (HCl, ACS reagent, fuming ≥37 wt%), and dichloromethane (DCM, CHROMASOLV®, suitable for HPLC, ≥ 99.8 %, containing amylene as a stabilizer) were purchased from Sigma Aldrich (Milano, Italy). Tetrahydrofuran (THF) (anhydrous, containing 250 ppm of BHT as an inhibitor, >99.9 %) was purchased from Merck (Milano, Italy). The metallic substrates (i.e., mild carbon steel and aluminum alloy) for coatings deposition were purchased by Q-Lab Corporation (Bolton, UK) in the form of a standard Q-panel (dimensions 76 mm × 152 mm × 0.64 mm). Mild carbon A100 steel substrates (type S) had a ground surface finish (0.81 mm thick; roughness = 0.51–1.14 μm) while aluminum alloy 3003 H14 panels (type A) had untreated smooth surface (0.64 mm thick; roughness <0.5 μm). Their nominal elemental composition is as follows. For A100 steel (SAE 1008/1010; ASTM A1008): Fe balance, Mn < 0.60 %, C < 0.15 %, S < 0.035 %, P < 0.03 %. For AA3003-H14 aluminum alloy (ASTM B209): Al balance, Mn 1.00–1.50 %, Fe < 0.70 %, Si < 0.60 %, Cu 0.05–0.20 %, Zn < 0.10 %, others 0.05–0.15 %. Tomato pomace was provided by TomatoFarm s.r.l. (AL, Italy), a tomato canning industry located in the north of Italy. Batches of fresh pomace (*i.e.*, by-product) were collected in proper plastic food packaging bags immediately after their production by the tomato processing plant (collecting periods: first week of September 2022 and 2023, respectively) and delivered to our labs the same day into closed and dark containers. Each seasonal batch (40–50 kg) is then immediately partitioned into smaller samples to be easily stored in a freezer (ca. –20 °C) to avoid microbial growth that would lead to the deterioration of the vegetable matrix over the subsequent months.

2.2. Methods and procedures for coating preparation

2.2.1. Tomato peel processing

The specified amount of tomato waste (2–3 kg at a time) was firstly

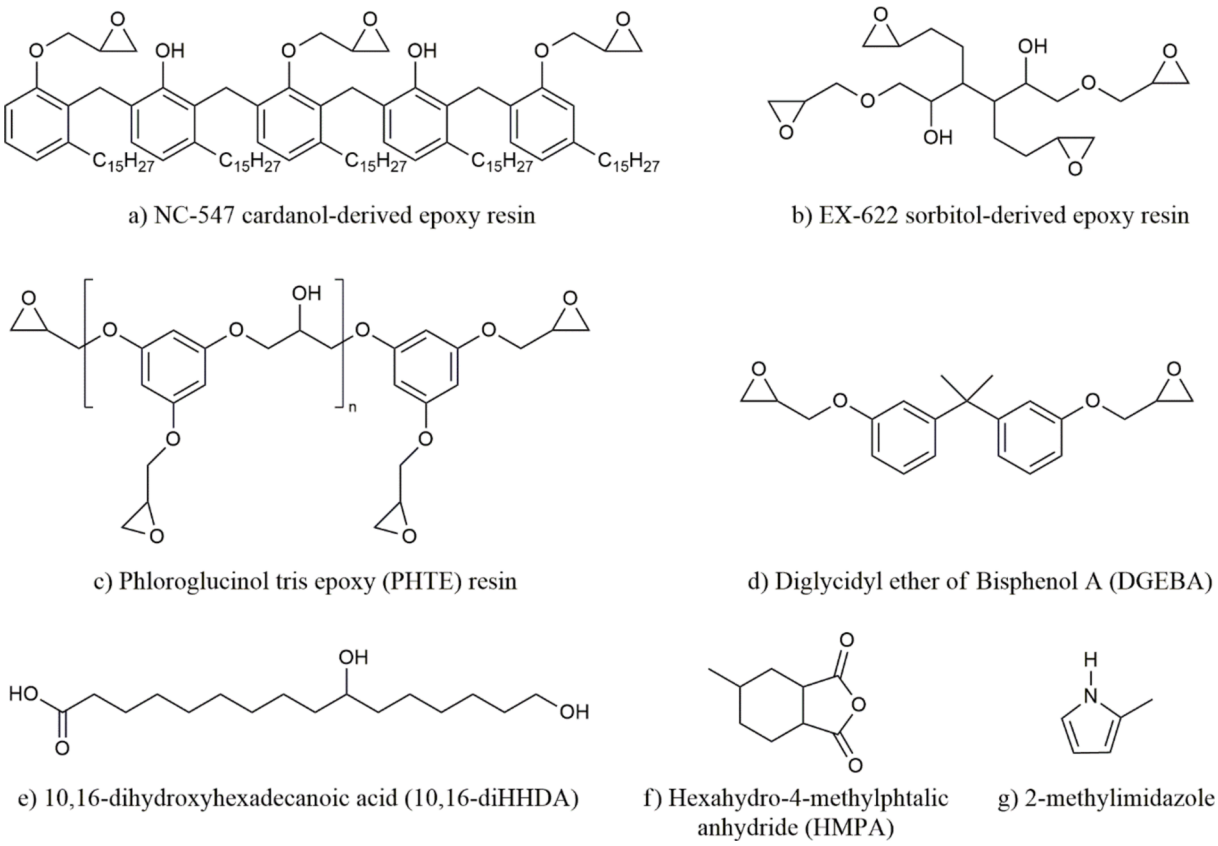

Fig. 1. Chemical structures of a) cardanol-derived epoxy resin (NC-547), b) EX-622 sorbitol-derived epoxy resin (EX-622), c) phloroglucinol tris epoxy resin (PHTE, n = 0.5–0.7), d) diglycidyl ether of Bisphenol A (DGEBA), e) 10,16-dihydroxy hexadecanoic acid (10,16-diHHDA), f) hexahydro-4-methylphtalic anhydride (HMPA), and g) 2-methylimidazole.

defrosted and then washed with water to separate seeds, which naturally sank to the bottom of the vessel, due to their higher density, from peels that remain on the water surface. The peels were then collected using appropriate tools, ensuring the removal of as much water as possible, and transferred directly to the oven for the drying process (60–80 °C, for approximately 2 days) necessary to stabilize the biological matrix. The dried peels were finely ground and stored in commercially available food packaging bags in the dark until their utilization. Approximately 100 g of dried tomato peels were degreased to remove the impurities called oleoresin fraction containing free fatty acids, waxy components, and carotenoids, which could interfere with the chemical processing of the biomass. This was achieved by subjecting the peels to Soxhlet extraction using n-hexane as a solvent for 6 h in a dynamic continuum process.

2.2.2. *Cutin depolymerization and 10,16-diHHDA isolation*

The molecule of interest is 10,16-diHHDA, which represents the most abundant monomer of cutin, the main structural component constituting the tomato peel. It was obtained from dried and degreased tomato peels (section 2.2.1) through a 4-step procedure. The first step consisted of the cutin depolymerization by alkaline methanolysis, using a modified version of the method proposed in the literature [37] that allowed to overcome important criticalities, thus significantly improving the purity and yield of the desired product. 30 g of defatted peels were placed into a round-bottomed flask and 300 mL of 1 M NaOH in MeOH (1:25, w/v) solution was added under vigorous magnetic agitation. The suspension was refluxed at 80 °C for 3 h, during which it turned a darker shade of orange, and then it was allowed to cool down to room temperature. Then, the suspension was filtered through a Büchner funnel diluting it with 600 mL of Water Milli-Q® water. While the solid residue was discarded, the filtered red solution was acidified by adding 37 wt% HCl until a pH = 3.5 was reached. While monomer precipitation occurs, the mixture becomes lighter, turning from red to yellowish. In the last step, the acidified mixture was divided into two aliquots for an easier work-up. Each part was carefully extracted into a separatory funnel with DCM (2 × 200 mL). The aqueous phase was then washed with DCM (1 x 100 mL) monitoring the success of the process by TLC analysis to verify the absence of monomer in the aqueous phase. Finally, all the organic phases were collected, and the solvent was stripped out through the rotary evaporator to obtain an orange wax-like material. The final product was 10,16-diHHDA with a purity of around 92 %, as evaluated by the gas chromatography-mass spectrometry technique. The overall yield over the four steps was 47 wt% on average considering the initial biomass waste, resulting in an average recovery of the 10,16-diHHDA of 67 wt%, evaluated on the weight of the dry residual corresponding to the non-hydrolizable biomass.

2.2.3. *Coating preparation*

All coatings were prepared without using any solvent. The curing agent (10,16-diHHDA (**e**) or compound (**f**)) and catalyst (**g**) were added into a beaker, heated at 90 °C, and mixed until well solubilized. Afterward, the selected epoxy resin (**a**-**d**) was added and stirred from 5 to 10 min to ensure a homogeneous mixing. The ratio between the moles of epoxy groups of the resin and those of the reactive hydrogen (*i.e.*, –OH and –COOH groups) of 10,16-diHHDA was varied together with the catalyst percentage and the curing parameters to tune firstly the glass transition temperature and the crosslinking degree of the cured coatings and then the resulting properties of some selected cured coatings. The moles of epoxy functional groups in the resins were calculated exploiting EEW reported in the technical datasheet of the resins (the average value of 700 g/eq was considered for NC-547; 189 g/eq for EX-622; 120.5 g/eq for PHTE; 170 g/eq for DGEBA). The reactive hydrogen equivalent

weight (RHEW) of the curing agents is 96 g/eq for the formulations cured with 10,16-diHHDA and 84 g/eq for the reference petrol-based curing agent HMPA (**f**). For 10,16-diHHDA as a curing agent, the actual RHEW was obtained by multiplying the theoretical one by 0.9, to consider the purity of the compound (see 2.2.2). The weight of the 2-methylimidazole catalyst was calculated to have a mole concentration of 3 %, 5 %, and 10 %, concerning the epoxy group moles. The fully bio-based mixtures were crosslinked at different curing conditions to maximize their crosslinking conversion and minimize curing time, e.g.,: i) PHTE and 10,16-diHHDA were cured in an oven at 150 °C for 2 h; ii) EX-622 and 10,16-diHHDA at 170 °C for 4 h; iii) NC-547 resin and 10,16-diHHDA at 180 °C for 6 h; iv) the petrol-based coating with DGEBA and HMPA was cured at 120 °C for 1 h. The different conditions for the curing treatment were selected considering unsuccessful previous tests of gelation and curing at lower temperatures and time values. Mixtures were either poured on polytetrafluoroethylene (PTFE) molds or glass or used to coat Q-panels of mild carbon A100 steel substrate and aluminum alloy 3003 H14 for assessing the adhesion strength and the corrosion protection properties of the thermosetting coatings. For all tests, the mechanically polished (ground) surface of the metallic panels (76 × 152 mm^2) was used. Materials cured on PTFE surfaces were employed for analysis by Fourier-transform infrared spectroscopy (FT-IR), differential scanning calorimetry (DSC), gel content measurements, and thermogravimetric analysis (TGA). Before the film application on metal and glass surfaces, all substrates were washed using 2-propanol, methanol, and acetone and dried with a nitrogen flux, to remove the residual organic impurities on the surface that could reduce the film adhesion. Hereafter, an air plasma treatment was performed to increase the substrate's surface energy. Substrates were treated for 60 s, using a discharge power of 150 W under an air atmosphere at a reduced pressure. A K202 Control Coater (RK Print Coat Instruments Ltd, Royston, Hertfordshire, United Kingdom) was used to deposit the coatings on substrates by bar coating technology using a bar with a close wound rod (wire diameter 1.20 mm) and a coating speed of 2 m/min. After curing, the coatings had an average thickness of 220 μm and an area of around 5 × 7 cm^2.

2.3. Characterization methods

2.3.1. FT-IR spectroscopy analysis

FT-IR spectroscopy was performed with a Fourier-Transform Infrared instrument named Nicolet 760-FTIR nexus spectrometer (Thermo Fisher Scientific, Waltham, Massachusetts, USA). FT-IR spectra were measured for KBr round tablets, obtained by pulverizing cured coatings and compressing them with KBr anhydrous powder. A preliminary background analysis was conducted to consider atmospheric effects before assessing any samples. FT-IR spectra were recorded from 4000 to 400 cm^{-1} with a resolution of 4 cm^{-1} and a scanning number of 64 times. Spectra analysis was done using OMNIC Specta Software (Thermo Fisher Scientific, Waltham, Massachusetts, USA).

2.3.2. Gel content measurements

A solvent extraction method was utilized to determine gel content (*Gc*) and evaluate the coating crosslinking degree. The sample was cured in a PTFE mold to facilitate its detachment due to the low adhesion to the fluorinated surface. Firstly, the initial weight of the coatings, m_0, was measured and the specimens were packed in filter paper. THF was added into a vial with a solid-to-liquid (g mL^{-1}) proportion ratio of 1:100. Coatings were dipped in THF and the solvent was stirred at 250 rpm for 24 h. The THF solution containing the solubilized part of the coatings was carefully transferred into a round bottom flask, dried by a rotavapor RV 8 (IKA, Staufen im Breisgau, Germany), and weighed In this work, *Gc* was calculated from the sol part, which was the coating extracted by THF from cured polymer networks, m_e, as follows:

$$Gc = 100 \bullet \left(1 - \frac{m_e}{m_0}\right) \quad (1)$$

At least three parallel tests for each sample were performed to report the gel content results as the average ± standard deviation values.

2.3.3. Differential scanning calorimetry (DSC)

Thermoanalytical analyses were performed using a DSC 283e (Mettler-Toledo, Columbus, Ohio, USA) instrument. Samples with masses of 5–20 mg were placed in 100 μl aluminum pans with punctured lids under a nitrogen atmosphere. The applied heating and cooling rate was 20 °C min^{-1}. The thermal behavior of the samples was investigated using the following thermal treatment: a heating ramp from −50 °C to 150 °C, a cooling step from 150 °C to −50 °C followed by a second heating step from −50 °C to 200 °C. The values of glass transition temperatures, determined as the inflection point of DSC profiles, were obtained from the second heating runs by averaging 3 measurements.

2.3.4. Thermogravimetric analysis (TGA)

TGA analysis was performed with a Q500 (TA Instruments, New Castel, Delaware, USA) instrument by heating from room temperature to 800 °C with a heating rate of 20 °C min^{-1} in air and nitrogen atmosphere. Degradation temperatures were taken as the temperatures at which the sample lost 5, 10, and 30 % of its mass.

2.3.5. Optical contact angle and surface energy measurements

Optical contact angle measurements were carried out using an OCA 15 plus instrument (Dataphysics Co., Filderstadt, Germany), equipped with a CCD photo-camera and a 500 μL Hamilton syringe to dispense droplets of testing liquids. Water supplied by LiChrosolv® was used, and the liquid droplet volume was 2 μL. Diiodomethane (purity 99 %, containing Cu as a stabilizer) was employed in a droplet of 1.5 μL. Measurements were performed at room temperature, using the sessile drop technique. The instrument software automatically evaluated contact angles by fitting the captured drop shape to the one calculated from the Young–Laplace equation. The resulting contact angle values were obtained on an average of 10 droplet measurements. Using the measured contact angles for the two different wetting liquids, surface energies of coatings were derived by using the Owens, Wendt, Rabel, and Kaeble (OWRK) method [38], using the following dispersive γ_d and polar γ_p components of the surface tension γ for water and diiodomethane: $\gamma_{d,H2O}$ = 19.9 mN/m; $\gamma_{d,CH2I2}$ = 47.4 mN/m; $\gamma_{p,H2O}$ = 52.2 mN/m; $\gamma_{p,CH2I2}$ = 2.6 mN/m.

2.3.6. Nanoindentation tests by atomic force microscopy (AFM)

Nanoindentation tests were carried out with an atomic force microscope AFM (NSCRIPTOR system provided with closed-loop sensors, which perform calibration and linearization of the piezo scanner in x, y, and z) driven by SPMCockpit software (NanoInk., Skokie, IL, USA) at room temperature, using commercially available silicon ACT probes purchased from AppNano (Santa Clara, CA) with a nominal spring constant k of 37 N/m, a conical tip and a half-opening angle of $\alpha = 24°$. Each probe was calibrated by performing a force–distance curve on a silicon wafer substrate, which can be considered as an infinitely hard substrate that cannot be indented by a silicon tip. Before the calibration, each silicon surface was cleaned by immersion for 30 min in piranha solution (1:3 mixture of H_2O_2 30 wt% and concentrated sulfuric acid), then rinsed with ultra-pure water, methanol, and blown dry with nitrogen. Substrates were also cleaned ultrasonically in ethanol for 15 min and dried with a nitrogen flux. Elastic modulus, k, of samples under investigation was obtained from the force–distance curves based on the Sneddon model [39], which related the deflection d and the indentation δ as follows:

$$kd = \frac{2}{\pi}\tan\alpha\left(\frac{E_s}{1-\nu_s{}^2}\right)\delta^2 \quad (2)$$

where E_s is the elastic modulus of the coating (assuming an infinitely higher modulus of the probe compared to the sample), ν_s is its Poisson ratio that was assumed to be equal to 0.35 for epoxy coatings with high cure degree [40,41]. Young's modulus values were calculated by fitting the Sneddon model to the curves in the region of reversible elastic deformations according to the method developed in a previous paper [42].

2.3.7. Scratch tests

The pencil hardness tests were performed according to BS EN ISO 15184:2020 standard [43]. Pencil scratch hardness was measured by imposing a mechanical load using pencil leads (KOHI-Noor Hardtmuth, Czech Republic) with an increasing hardness. The reported hardness corresponded to the hardest pencil that did not scratch the surface.

2.3.8. Adhesion pull-off tests

Pull-off tests were performed by gluing a metallic dolly with a bicomponent epoxy resin Araldite 2011 (Huntsman, Salt Lake City, Utah, United States) to the coated samples. A plasma pre-treatment was performed both for coatings (190 W, 5 min, air atmosphere) and dollies (190 W, 15 min, air atmosphere) to promote glue adhesion. After a complete curing of the glue, dollies were clamped and pulled with increasing pressure. When the dolly detached the film from the substrate, pull-off pressure was measured. Tests were performed according to BS EN ISO 4624:2016 standard [44], with a manual self-aligning tester ARW-T05 (ARW Misure, Zanè, Vicenza, Italy), and at least three dollies per coating were applied.

2.3.9. Colorimetric analysis

For color analysis of coatings, the light reflected from the coated sample is measured with a YS3010 Spectrophotometer (3nh, Guangzhou, P.R.China), exploited to determine L*, a*, b* values in CIELab space, with an observation angle of 8° and a standard light D65 as a light source.

2.3.10. Electrochemical investigation of coated steel specimens

The corrosion protection performance of each type of cured coating was assessed through an electrochemical investigation of the related steel-coated sample. Each specimen was tested at a minimum of two spots (used area per each test: ca. 6 cm^2). If results were not sufficiently similar, a third and even a fourth fresh spot was tested to improve the reliability of the data set. A three-electrode configuration was used in each testing protocol, with the coated steel plate used as the working electrode, a platinum wire (approximate geometric area 1.5 cm^2) as the counter electrode, and an AgCl/Ag electrode (in aqueous 3 M KCl) used as the reference one. The electrodes were properly arranged in a glass cell with a hole 1 cm in diameter in the bottom part. Each coated sample was sealed to the cell using a bi-adhesive tape 0.5 mm in thickness (A2 Soluzioni Adesive, Italy). A 2.5 × 2.5 cm^2 square of tape with a 10 mm hole in the middle was attached to the coated sample and pressed tightly against the flat bottom surface of the cell to ensure the two surfaces were sealed. Then, the cell was filled with approximately 100 mL of naturally aerated, near-neutral NaCl 3.5 wt% solution, replicating a seawater environment. To minimize ohmic drop, the reference electrode was placed into a glass Luggin capillary, and its tip was carefully positioned as close as possible to the approximately 0.78 cm^2 spot of the coated steel. The assembled cell was placed inside a homemade Faraday cage to shield the apparatus from external electromagnetic interference. Electrodes were finally connected to a potentiostat/galvanostat/ZRA instrument (Interface 1000; Gamry, USA) run by a PC through the Gamry Frameworks software (Gamry, USA). For comparison, a pristine (i.e., uncoated) steel Q-panel was also tested. The protocol specifically developed for the electrochemical tests (Fig. 2), aimed at quantitatively monitoring the coating features as a function of its formulation, integrates a first natural aging period with a modified version of the Accelerated Cyclic Electrochemical Technique (ACET), an ISO

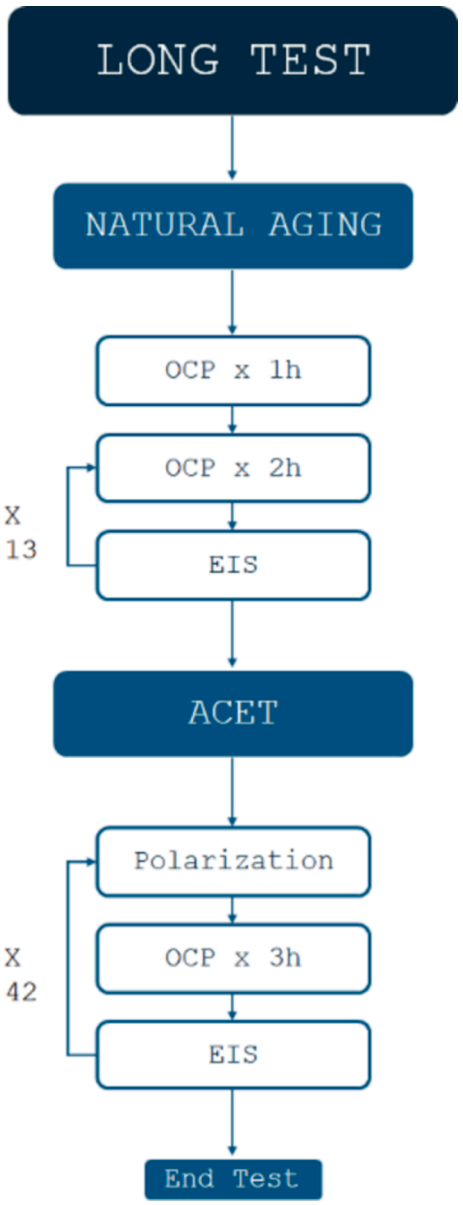

Fig. 2. Block diagram of the electrochemical protocol adopted to assess quantitatively the performance of the coatings towards the corrosion protection of metal specimens.

procedure coded for assessing the effectiveness of industrial paint and coatings for metals and alloys [45]. ACET is constituted by a three-step method that includes, in sequence, i) potentiostatic polarization (*i.e.*, aging step), ii) open circuit potential monitoring (i.e., relaxation period), and iii) electrochemical impedance spectroscopy (EIS) measure. According to the ISO method, the sequence must be successfully repeated up to 6 times to confirm the good adhesion and the satisfactory protection of the coating. In this study, the cyclic protocol was repeated 42 times, resulting in a much more severe aging condition that lasted for seven times longer than the period suggested by the standard procedure. The total duration of the accelerated test is approximately 7 days. The experimental details of the entire experimental protocol are as follows. After an initial equilibration period lasting two hours, during which the open circuit potential (OCP) was monitored, the natural aging period began. It lasts around 1 day and was obtained by repeating 13 times the following two-step protocol: i) OCP monitoring for one hour and ii) EIS investigation, by recording spectra at the established OCP by applying a 10 mV (rms) amplitude sinusoidal perturbation signal with a frequency

scanned within the range 100 kHz – 10 mHz (ten points per decade, logarithmically distributed). Then, the accelerated aging period started, lasting one week. It includes: i) potentiostatic polarization, performed for 20 min by setting a potential of – 4 V vs. AgCl/Ag (double the minimum potential reported in the ISO method); ii) OCP of the relaxing system, monitored for 3 h after the end of the polarization step; iii) EIS spectra, recorded as described above.

3. Results and Discussion

3.1. 10,16-diHHDA extraction and preliminary screening of bio-based epoxy resins

The trifunctional monomer 10,16-diHHDA was obtained with an average purity of 92 wt% and recovery efficiency of 67 % through the depolymerization of cutin present in tomato peels discarded by the canning industry. This is the best performance reported in the literature (Table S1). As our previous studies stated [12,16], the highly pure bio-derived 10,16-diHHDA is a waxy solid, stable in air at room temperature and without any unpleasant odor. All these features made the monomer handling and storage easy and user-friendly. Moreover, the high purity of the cutin monomer enabled the successful curing of 10,16-diHHDA with epoxidized precursors for the first time, excluding any synergistic effect from the components co-present in the previously reported tomato extracts [18,19].

To explore the effect of using the tomato cutin monomer as a curing agent of epoxy coatings, several bio-based coating formulations were prepared in a preliminary phase of this study, combining 10,16-diHHDA with different epoxy resins obtainable from renewable sources, such as NC-547 that is an epoxidized cardanol-based resin, EX-622 that is a sorbitol-derived epoxy resin, and PHTE that is a phloroglucinol tris epoxy resin. The fully bio-based coatings were cured and compared to a reference fossil-based coating obtained from curing DGEBA resin with HMPA, used as a benchmark. Other possible comparisons with coating references obtained by combining DGEBA with 10,16-diHHDA and bio-based epoxidized resins with HMPA were unfeasible due to the solubility issues of reactants. Among the many variables influencing a metal protective coating, glass transition temperature (T_g) is a key property that can be easily determined experimentally. Effective coatings should have a T_g higher than the temperature at which they can be exposed in operating conditions, e.g. at least higher than room temperature.

The glass transition temperature values of the newly developed bio-based crosslinked coatings were assessed using DSC profiles and are listed in Table 1. In this preliminary screening, the stoichiometric ratio between epoxy groups and hydrogen active nucleophiles (–XH), *i.e.*, –OH and –COOH, of curing agents, was kept equal to 1:1 as well as the concentration of 2-methylimidazole was fixed at 3 mol% to catalyze the reaction. Different curing conditions were used due to the diverse chemical nature of the resins.

Cardanol-based NC-547 coating showed a glass transition temperature lower than the others, and the sorbitol-based EX-622 coating exhibited a T_g still lower than room temperature. Only the coating with PHTE showed a glass transition temperature comparable to room temperature but still too low for any practical application as protective coatings. For this reason, PHTE was selected as the most promising bio-based epoxy resin for further development tests aiming at increasing T_g and approaching the T_g values of DGEBA-based coatings used as a benchmark.

Table 1
Glass transition temperature, T_g, compositions of the liquid mixture, and curing conditions employed for preparing the fully bio-based coatings and reference fossil-based coating developed during the preliminary screening. In all cases, a 3 mol.% constant concentration of 2-methylimidazole was used as a catalyst.

Resin	Curing agent	Epoxy: X–H molar ratio	Curing conditions	T_g (°C)
NC-547	10,16-diHHDA	1:1	6 h, 180 °C	−5 ± 2
EX-622	10,16-diHHDA		4 h, 150 °C	6 ± 2
PHTE	10,16-diHHDA		2 h, 150 °C	25 ± 10
DGEBA	HMPA		1 h, 120 °C	130 ± 1

3.2. Effect of epoxy resin/X–H molar ratio and catalyst concentration on crosslinking degree and glass transition temperature

In the presence of 2-methylimidazole, the –COOH groups of 10,16-diHHDA can be esterified by their reaction with epoxy groups, forming a secondary –OH group. Also, the primary and secondary –OH groups of 10,16-diHHDA can be etherified by their reaction with epoxy groups, producing other secondary OH groups. These secondary –OH groups formed can further react with other epoxy groups producing branches and ramifications [46]. To obtain densely crosslinked coatings with high T_g values and corrosion metal protection, the reaction of secondary OH groups was exploited to increase the number of crosslinking points in newly developed bio-based coatings. For this reason, the effect of an increased epoxy/curing active groups ratio on the T_g coatings was studied and various compositions based on PHTE were investigated, varying the molar ratio between reactive groups and the catalyst percentage, to increase the T_g and anti-corrosion properties of the cured PHTE-based coatings. The epoxy group:X–H ratio was progressively increased from 1:1 to 8:1, while the catalyst percentage varied from 3 and 10 mol.%, in the case of the 2:1 ratio, and from 3 to 5 mol% in the case of the 4:1 and 5:1 ratios. From here on, samples will be referred to as AB_x:y_z, where A identifies the epoxy resin (P for PHTE; D for DGEBA used as petrol-based reference), B represents the curing agent (C for 10,16-diHHDA; M for HMPA), x:y defines the epoxy group:X–H ratio and z corresponds to the catalyst concentrations (in mol.%). For example, the coating made of PHTE and 10,16-diHHDA with an epoxy group:X–H ratio of 2 and 3 mol.% of catalyst is named PC_2:1_3. The results in terms of glass transition temperatures and crosslinking degrees, determined by DSC analyses and gel content measurements, respectively, are listed in Table 2. As mentioned in section 2.3, the second heating ramp was considered for T_g evaluations, because the first ramp has the purpose of erasing the previous thermal history. Table 2 shows that T_g values of coatings cured with the lower amount of catalyst (3 mol%) increased by increasing the epoxy group:X–H ratio, up to the 5:1 ratio formulation reaching an average value of 77 °C.

Increasing the catalyst amount from 3 to 5 mol% consistently increased T_g, while maintaining a constant relative amount of epoxy vs. curing agent. A further rise in the catalyst (10 mol%) did not produce any additional improvement in T_g. The T_g increment is more evident by increasing the percentage of epoxy resin, with the 4:1 and 5:1 formulations with 5 mol% of catalyst, exceeding the threshold of 100 °C.

Table 2
Glass transition temperatures, T_g evaluated from DSC ramps and gel content (*Gc*) for the reference petrol-based coating with DGEBA (D) and HMPA (M) and the different fully bio-based PHTE-containing coatings, as a function of the formulation.

Sample	Epoxy group:X–H ratio	Catalyst conc. (% mol.)	T_g (°C)	Gel content (*Gc*) (%)
DM_1:1	1:1	3	130 ± 1	93 ± 2
PC_1:1_3	1:1	3	25 ± 10	96 ± 1
PC_2:1_3	2:1	3	35 ± 4	97 ± 2
PC_2:1_5	2:1	5	78 ± 8	96 ± 3
PC_2:1_10	2:1	10	55 ± 4	97 ± 2
PC_4:1_3	4:1	3	59 ± 11	98 ± 1
PC_4:1_5	4:1	5	104 ± 12	98 ± 1
PC_5:1_3	5:1	3	77 ± 12	99 ± 1
PC_5:1_5	5:1	5	104 ± 9	99 ± 1
PC_6:1_3	6:1	3	74 ± 2	99 ± 1
PC_8:1_3	8:1	3	47 ± 2	99 ± 1

Compared to the petrol-based DM_1:1 coating, all bio-based samples still have lower T_g values. However, an improvement is evident for samples PC_4:1_5 and PC_5:1_5, reaching a value of just 10–15 °C lower than the reference BPA-containing resin.

The cross-linking degree estimated by gel content measurements was high in all PHTE samples with no significant effect of the catalyst amount and the epoxy resin/curing agent ratio on the selected materials. This finding indicates that all formulations ensured a complete reaction of the reactive species.

Results presented in Table 2 were used to select a restricted ensemble of samples that were further characterized to elucidate correlations between the composition and properties of the thermosetting polymer. The effect of epoxy vs. curing agent was studied by selecting 2:1, 4:1, and 5:1 molar ratios, while the influence of catalyst concentration was analyzed by comparing PC_4:1_3 with the PC_4:1_5 sample. For the latter comparison, a 4:1 ratio was preferred to 5:1 because the PC_5:1_5 sample, while exhibiting a high T_g, showed a too-high reactivity in the liquid formulation that could cause premature crosslinking before the deposition on the substrate.

3.3. FT-IR spectroscopy and thermal resistance of bio-based coatings

Fig. 3 shows the IR spectra of the selected materials, where the following peaks can be attributed to: $–CH_2$ asymmetric and symmetric stretching vibrations (2862 and 2921 cm^{-1}, respectively); C=O stretching of ester groups at 1730 cm^{-1}, indicating the successful reaction of the epoxy resin with the carboxylic groups of 10,16-di HHDA; ring carbon–carbon stretching vibrations of aromatic rings at 1600 cm^{-1}; asymmetrical stretching vibration of aryl alkyl ether (C-O-C) peaks between 1294 and 1182 cm^{-1}; and ring vibrations of residual epoxy groups (908 cm^{-1} and 768 cm^{-1}, Fig. 2b) [47]. The peaks in the range 3100–3700 cm^{-1} can be attributed to unreacted –OH groups, probably due to the poor mobility of hydroxyl groups in the PHTE resin backbone. The coating with 5 % mol. of catalyst (PC_4:1_5) exhibited no peaks at 908 cm^{-1} denoting the absence of unreacted epoxy groups in this sample, despite their excess in the resin. The absence of IR absorption can be due to their reaction of epoxy groups with 2-methylimidazole introduced with a higher amount in this sample [48].

To assess the thermal resistance of the newly developed crosslinked materials, TGA analyses were performed, and Fig. 4 shows the TGA results obtained using both an atmosphere of nitrogen and air.

All the crosslinked materials appeared significantly more stable than the 10,16-diHHDA monomer itself. Higher degradation temperatures achieved for coatings suggest that a polycondensation reaction between –OH and –COOH groups of the cutin monomer may take place in 10,16-diHHDA sample because the initial loss of 10,16-diHHDA weight, noticed from 150 °C to 350 °C, was probably due to water loss induced by polycondensation and this could no longer happen when –OH and –COOH groups have reacted with PHTE. All the crosslinked samples followed a similar degradation pattern, with a decomposition temperature at 5 % of weight loss ($T_{5\%}$) of around 340 °C in air and 345 °C in nitrogen atmosphere. The main degradation temperature, where losses of 10 % and 30 % occurred, was around 354 °C and 378 °C in air and nitrogen atmosphere, respectively. Under the nitrogen atmosphere, only one major degradation phenomenon took place with a high charring residue of around 30–35 % of the initial mass (Fig. 4a). This was probably due to the PHTE trifunctionality, which can theoretically increase the coating crosslinking density when compared to DGEBA and thus reduce the possibility of producing volatile fragments during the thermal decomposition process [49,50]. Also, compared to bio-based coatings, the DGEBA-based sample showed a higher total weight loss of nearly 10 % and a weakly higher thermal resistance, likely due to higher thermal resistance of the cycloaliphatic HMPA used as a curing agent for DGEBA. PC_2:1_3 material with a higher amount of cutin monomer showed a total weight loss slightly higher than the other cutin-based materials and lower than 10,16-diHHDA. This could indicate that the presence of PHTE significantly enhanced the thermal stability of the material. On the other hand, no final residue was observed in an oxidative atmosphere for materials under investigation, due to the occurrence of a complete degradation in air. Two main degradation temperatures of about 366 °C and 580 °C were noticed, with a corresponding weight loss of 55 % and 43 %, respectively (Fig. 4b).

3.4. Wettability and surface energy analysis of bio-based coatings

The surface wettability of the newly developed coatings was determined by measuring the optical contact angles using water and diiodomethane as wetting liquids, as depicted in Fig. 5. The contact angle measurements were employed to determine the total surface energies and their corresponding dispersive and polar components (Table 3).

Fig. 5 shows that all the coatings can be considered hydrophobic, with an average contact angle with water slightly higher than 90°. The left and right angles were similar for all the samples, as shown for example for PC_5:1_3 in Figure S1. Comparable values of contact angles were measured on aluminum substrates (Figure S2). Moreover, all bio-based coatings exhibited a more hydrophobic behavior than the petrol-based DM_1:1, especially using steel as a substrate, probably due to the presence of the long aliphatic linear chain of 10,16-diHHDA that increased dispersive and apolar interactions. Contact angle values were used for determining surface energies of the selected coatings on steel and aluminum, by employing the OWRK method (Table 3 and Table S2). The surface energies of all coatings are around 35 mN/m, and the dispersive components are significantly higher than the polar ones. These low values for surface energy polar components indicate a

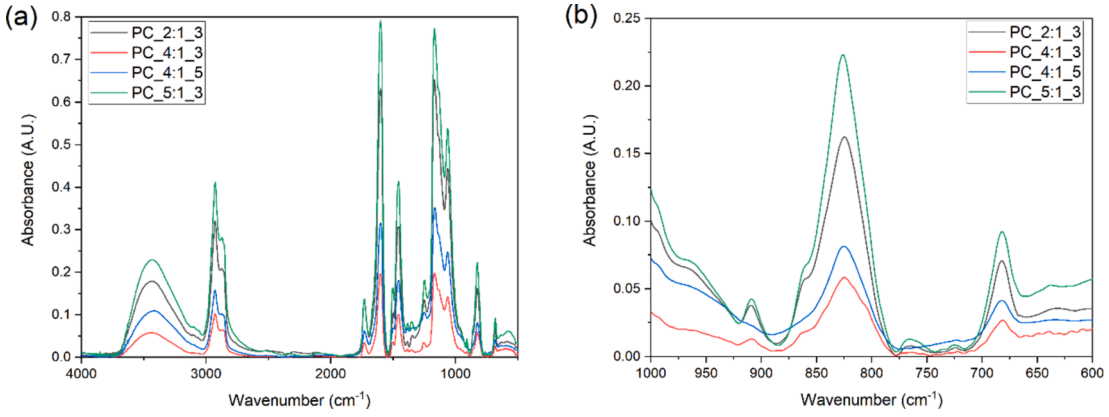

Fig. 3. (a) Full-range and (b) selected-range FTIR spectra of the crosslinked materials obtained with different epoxy: H active nucleophile ratios obtained from PHTE (P) and 10,16-diHHDA (C) and with different percentages of 2-methyimidazole as a catalyst (3% and 5% mol.).

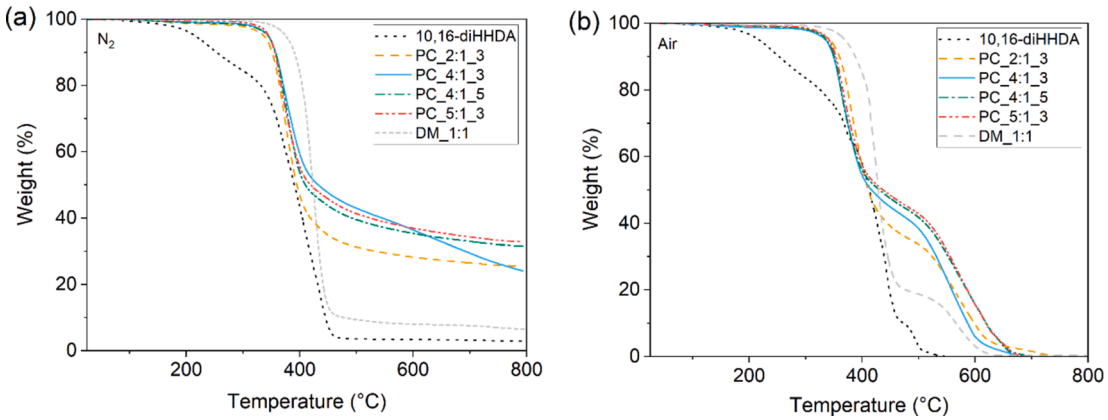

Fig. 4. Thermogravimetric analysis of samples with different molar ratios between epoxy groups and H active nucleophiles obtained from PHTE (P) and 10,16-diHHDA (C) and with different weight percent of 2-methyimidazole as catalyst (3% and 5% mol.), reference petrol-based sample obtained with DGEBA (D) and HMPA (M) and pure 10,16-diHHDA, under a nitrogen atmosphere (a) and air (b).

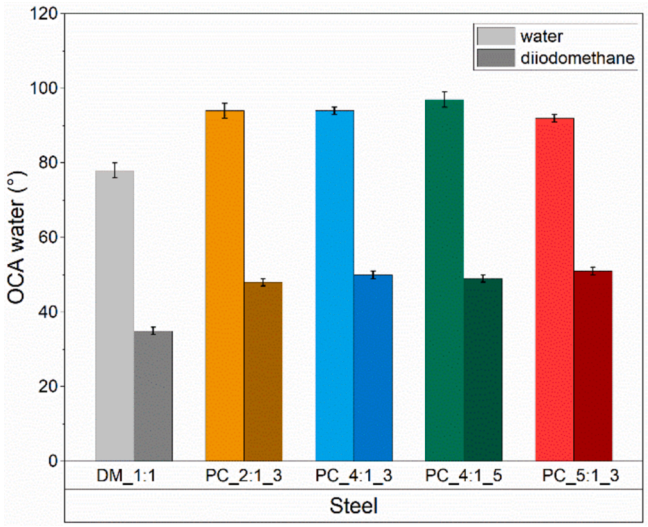

Fig. 5. Optical contact angle values measured using water (light colors) and diiodomethane (dark colors) as wetting liquids for cutin-based coatings deposited on steel substrates and obtained with different epoxy:X–H molar ratios obtained from PHTE (P) and 10,16-diHHDA (C) and with different molar percentages of the catalyst (3% and 5% mol.), reference petrol-based sample obtained with DGEBA (D) and HMPA (M).

Table 3
Values of total surface energies (γ), with their dispersive (γ_d) and polar (γ_p) components, according to the Owens-Wendt-Rabel-Kaelble (OWRK) method, for petrol-based reference and cutin-based coatings deposited on steel substrates and obtained with different epoxy:X–H molar ratios and with different molar percentages of catalyst.

Coating	γ (mN/m)	γ_d (mN/m)	γ_p (mN/m)
DM_1:1	42.2	36.9	5.3
PC_2:1_3	35.1	34.1	1.0
PC_4:1_3	34.1	32.9	1.2
PC_4:1_5	34.4	33.8	0.6
PC_5:1_3	33.5	31.6	1.9

repulsion of the coating surface towards polar liquids. This could be beneficial for reducing the water penetration inside coatings and enhancing corrosion resistance.

3.5. Mechanical and technological properties of bio-based coatings

To assess the mechanical properties of the selected coatings which are not self-standing films and were deposited on steel and aluminum substrates, Young's moduli were measured by AFM nanoscale indentation tests by employing the Sneddon model, as explained in Section 2.3. Moreover, coating hardness and adhesion strength were respectively determined by technological pencil tests and pull-off tests. The results are listed in Table 4.

Table 4 shows that the elastic modulus did not appear to be affected by the amount of 10,16-diHHDA present in the coatings. An average elastic modulus of approximately 3.0–3.5 GPa for all coatings was obtained except for PC_5:1_3, which showed a significantly lower value. However, similar values of 2–3 GPa were found for conventional filler-free coatings obtained by curing petrol-based epoxy resins [51] and the inhomogeneity in the modulus could be due to measurement AFM artifacts, caused by some variations in the tip–sample contact area [52].

Regarding the levels of coating hardness, the results of pencil scratch tests (Table 4) reveal a difference among the four coatings examined in this paper. An increase of epoxy:X–H molar ratio led to an increase in hardness till a maximum of 3H, obtained for both PC_4:1_3 and PC_5:1_3 cured with a 3 % mol. of catalyst. This hardness level can be further improved by increasing the percentage of catalyst from 3 % to 5 % mol., as confirmed by PC_4:1_5 with a higher hardness level of 5H. This increase in hardness can be due to the reaction of 2-methylimidazole with the epoxy groups of the resin (see also spectra evidence in section 3.3), stiffening it. Since the heterocycle is monofunctional, it will only lead to stiffening of the coating due to its rigid structure. In this case, 2-

Table 4
Young's modulus from force-distance curves performed by AFM, average results of pencil hardness tests performed on the materials deposited on steel, and aluminum, and pull-off strengths measured for cutin-based coatings deposited on steel and aluminum substrates and obtained with different epoxy:X–H molar ratios and with different molar percentages of catalyst.

	Thickness (μm)	Young's modulus (GPa)	Pencil hardness	Pull-off Strength (MPa)	
Substrate	Steel and Aluminum			Steel	Aluminum
PC_2:1_3	204 ± 18	3.3 ± 1.4	HB	1.1 ± 0.3	0.8 ± 0.1
PC_4:1_3	209 ± 19	3.2 ± 0.5	2H – 3H	1.0 ± 0.1	0.6 ± 0.1
PC_4:1_5	243 ± 28	3.8 ± 0.4	4H – 5H	1.4 ± 0.1	1.2 ± 0.2
PC_5:1_3	248 ± 34	1.4 ± 0.2	3H	1.3 ± 0.1	1.1 ± 0.1

methylimidazole at higher concentrations not only acted as a catalyst, but also as a substrate, leading to a more rigid and stiff coating.

The pull-off strength values in Table 4 revealed a fairly good adhesion of the coatings under investigation, both on aluminum and steel substrates. By comparing the cutin-based coatings, an increase in the molar ratio appeared to cause an improvement in adhesion. An excess of epoxy and hydroxyl groups in coatings with high molar ratios, free to react and bond with the substrate, could contribute to improving adhesion. Also, an increase in catalyst percentage is beneficial to enhance the adhesion both towards steel and aluminum substrates. In any case, the adhesion can be further increased using either a primer or a substrate silanization pretreatment in future industrial applications.

A yellowing-reddish color was observed for all the bio-based coatings with slight color differences caused by different thicknesses (Figure S3 and S4), although the average thickness of the examined coatings is around 220 μm (Table 4).

3.6. Electrochemical characterization of coatings

Electrochemical investigation of coated conducting substrates is a valuable way to obtain quantitative information on the barrier effect towards the penetration of electrolyte solutions within a cured resin or paint, also in a time-resolved manner. The protection performance of insulating coatings can be obtained *in operando* conditions, by simply placing the coated specimen in contact with a solution that mimics the real exposure environment.

3.6.1. Corrosion protection performance

Electrochemical impedance spectroscopy (EIS) is a technique largely employed in the characterization of coated metals and alloys as it provides information not only on the occurrence of corrosion but also on key features of the coatings. Fig. 6 shows the Bode modulus plot with the spectra of the selected phloroglucinol-based coatings (PC_2:1_3; PC_4:1_3 and PC_4:1_5; PC_5:1_3) together with that of the pristine, uncoated steel plate and of the benchmark coated sample (DM_1:1). Impedance spectra were recorded after 3 h of immersion in the test solution electrolyte, a time sufficient to reach a steady-state condition as judged from the open circuit potential (OCP) curves (Figure S5).

The spectra of all samples showed a one-time constant process, with a characteristic time shorter for the uncovered sample. The impedance modulus spectrum of the bare steel looks different from that of any covered sample. It has a relatively flat section in the high and middle-high frequency region (a few tens of ohms, due to the uncompensated resistance of the electrolytic solution). This is followed by an increase in impedance modulus, indicating the occurrence of a faradic process at

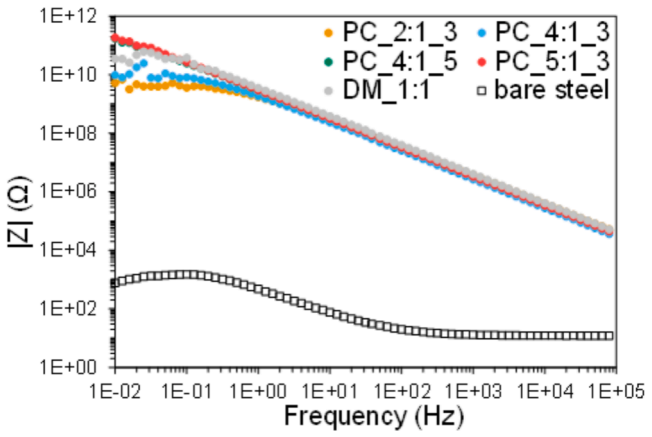

Fig. 6. Bode modulus plot of the phloroglucinol-based coatings. For the sake of comparison, petrol-based reference coating (DM_1:1) and bare steel are also reported.

the metal|electrolyte interface (i.e., metal corrosion), which is characterized by a time constant of hundreds of milliseconds. On the contrary, the coated samples invariably show a predominantly capacitive behavior, due to the dielectric nature of the coatings, with neatly higher impedance values (tens of GΩ cm^2 at the lower frequencies) and slower time constant (seconds scale) compared to those of the bare steel, pointing to an effective electrical insulation of metal surface by the polymer coating that acts as physical barrier towards electrolyte permeation. Among the bio-based formulations, coatings PC_4:1_5 and PC_5:1_3 exhibited better corrosion protection performance due to a more pronounced capacitive behavior (i.e., constant increase of $|Z|$ extends at lower frequencies) and higher values of the impedance modulus at the lowest frequency (i.e., $|Z|_{0.01\ Hz}$ ca. 100 GΩ cm^2). The metal|coating|electrolyte constitutes a quite dynamic system. The protective layer can change due to water uptake, diffusion of water and ions within the polymer matrix, and partial delamination of the coating. These processes can lead to localized corrosion. As the intensity and the speed of appearance of each of these detrimental processes are affected by the properties of the coating, it is essential to carry out their comparison by monitoring the systems over time, to obtain indications that can predict how the system will behave over a longer period and to identify any difference in behavior among the coatings.

The effect of natural aging on the coatings was assessed by recording, every hour, EIS spectra at OCP for around one day of exposure to the NaCl solution (Fig. 7).

To rationalize the behavior, each coating at every given soaking time was parametrized by many figures of merit selected from the ones proposed over the years to describe insulating coatings [53]. The parameters can be obtained either graphically, directly from the spectra ($|Z|_{0.01\ Hz}$, breakpoint frequency (f_b), breakdown frequency (f_{bd}), the frequency at the minimum phase angle (f_{min}), Damage Function) [54], or by fitting each whole spectrum with an equation describing the impedance response of a proper equivalent electric circuit [55]. The latter, in the specific case, is constituted by a parallel connection of a resistor (R_p), accounting for the pore resistance of the coating (i.e., polarization resistance), and a constant phase element (CPE) from which the coating capacity (C_{coat}) can be derived [56]. Looking at Fig. 7, the range of frequencies within which the system exhibits a resistive behavior (i.e., almost constant $|Z|$ values and ca. 0° phase angle) invariably expanded for all cutin-derived coatings with the increase of the soak time. A lower variation was detected for the reference coating (Figure S7). Concurrently, $|Z|_{0.01\ Hz}$ and the related pore resistance R_p (being the solution resistance negligible) constantly decrease as well as C_{coat} increases (Fig. 8). Both evidences point out the occurrence of solution uptake by the polymer layer that results in more ionically conductive channels and an increase of the apparent dielectric constant of the layer, considering that water has a significantly higher relative permittivity than that of the polymer (80 and ca. 4–8, respectively). By coating capacitance, evaluated at the beginning of the test ($C_{coat,0}$) and at any subsequent residence time (C_{coat}), the Brasher-Kingsbury equation:

$$\varphi = \frac{log(C_{coat}/C_{coat,0})}{log\varepsilon_0} \quad (3)$$

where ε_0 is the dielectric constant of water, allows to quantitatively estimate the amount and the rate of solution ingress within the layer through the volumetric water uptake (φ), which represents the percentage of volume occupied by the solution within the polymer matrix (Fig. 8). It is important to highlight that these numbers have just a relative validity, as $C_{coat,0}$ is not referred to the dry coating but to the first available data, recorded after 3 h of exposure to the solution during which solution could have already entered the polymer layer.

Water uptake constantly increases over time and the process is not significantly affected by the amount of curing agent or catalyst, in good agreement with the comparable contact angle, surface energy, and gel content values. For the sake of comparison, the petrol-based coating

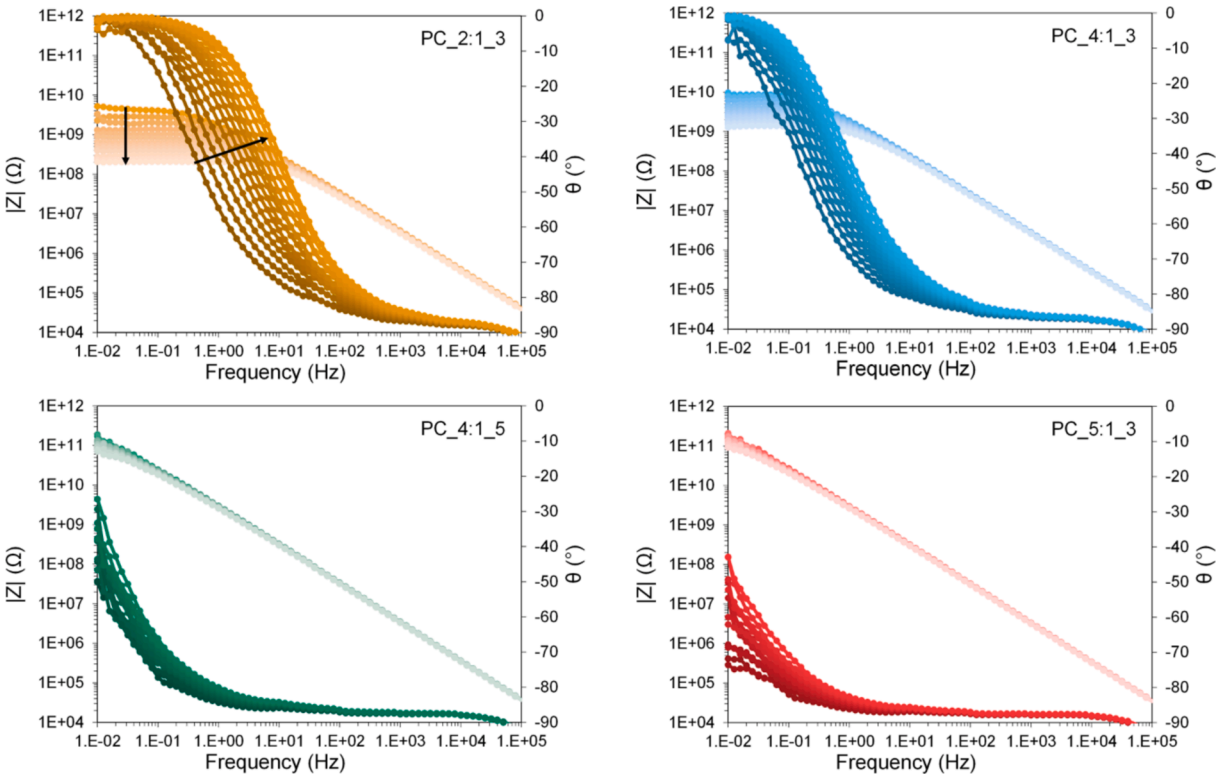

Fig. 7. Representative Bode modulus (left Y-axes) and Bode phase (right Y-axes) plots depicting the time evolution of the EIS spectra for the phloroglucinol-based coatings over 23 h of soaking into the working solution. Time resolution: 1 h. Arrows represent the time evolution of the spectra. For the sake of clarity, spectra have been gently smoothed. Raw spectra are shown in Figure S6 for completeness.

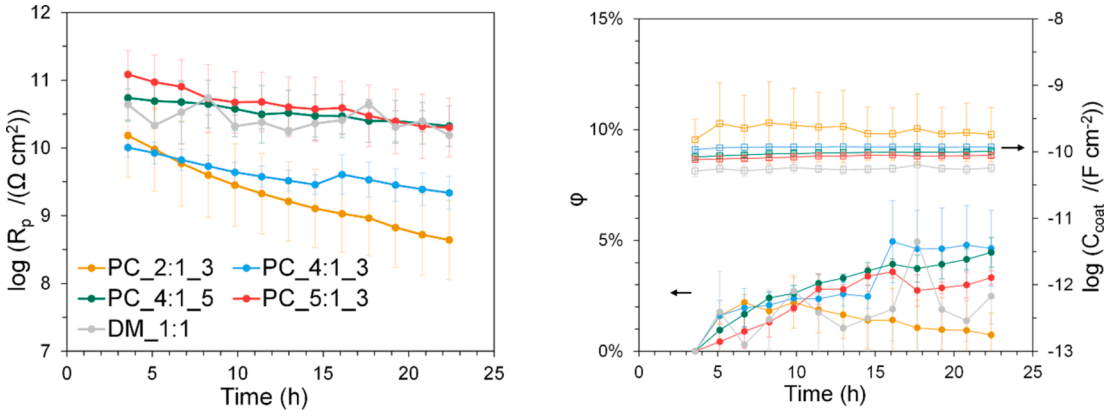

Fig. 8. Left: pore resistance (R_p) and right: relative volumetric water uptake (φ; full circles) and coating capacitance (C_{coat}; empty squares). Data are derived by EIS spectra recorded during the natural aging stage for the bio-based and reference coatings.

DM_1:1 shows lower values of C_{coat} but a similar amount and rate of water uptake during the considered exposure time. Accordingly, notwithstanding the improved hydrophobicity compared to the reference coating (Fig. 5), due to the aliphatic chain of the cutin monomer, its length could determine a bigger free volume among the crosslinked chains that can be easily filled by the solution during the exposure time. Relative volumetric water uptake after one day of exposure is below 5 % and, considering that no corrosion phenomenon is observable by the spectrum in any coatings, the solution reached only the outermost layer. Interestingly, PC_2:1_3 shows quite different behavior. Coating capacitance, and water uptake, show a first fast increase, up to around 8 h of immersion, followed by an evident decrease. This unique peak-shape trend could be explained by a more pronounced swelling phenomenon induced by water penetration that causes an increase in the apparent volume (and thickness) of the coating and hence a decrease of the detected capacitance and the related volumetric water uptake.

3.6.2. *Corrosion protection performance under accelerated aging*

Over time coatings undergo deterioration processes that lead to a progressive loss of their protection performance (e.g., deeper water penetration, detachment by the substrate). As the process often requires months or years before being observed, over time various protocols have been proposed to speed up the natural aging process of coatings to quickly obtain valuable predicting information on the long-term stability of coatings. One of these aging methods, based on instrumental analyses that can provide quantitative comparative data, has been stated as Accelerated Cyclic Electrochemical Technique (ACET). It was first proposed in the scientific literature [57,58] and then validated as a

standard control technique, coded as ISO 17463 [59]. The accelerated aging process is induced by stressing the organic coating using a cathodic polarization that triggers a hydrogen evolution reaction to occur at the wet metal surface reached by the solution possibly permeated through the polymer layer. The mechanical action of the electrogenerated gas bubbles, combined with pH change, can speed up the detachment of the coating from the substrate failing metal corrosion protection. Even if the trends of polarization currents, together with those of the open circuit potentials recorded during the relaxation stage of each ACET cycle, could provide qualitative information to evaluate the performance of the coating, the most valuable and quantitative information could be obtained by the analysis of EIS spectra.

The performance of all four bio-based coatings proves to be satisfactory under stressful conditions, showing pore resistance (R_p) exceeding 1 GΩ cm^2 after one week of accelerated aging testing. Notably, this key performance indicator is higher than those of similar bio-derived coatings previously documented in the literature (Table S3). It is important to emphasize that the referenced literature data were obtained in natural aging conditions rather than the highly demanding conditions associated with the accelerated aging test conducted in this study. Even under less demanding conditions, analogous bio-based coatings consistently exhibited lower pore resistance, ranging from a few kΩ cm^2 to 500 MΩ cm^2. Moreover, the latter value was obtained with a "mixed type" coating, with only one component of the formulation being bio-derived [18]. Furthermore, a comprehensive and detailed compendium of sustainable coatings and their corresponding performance metrics has been recently published [60].

Even if a benchmark threshold value for the identification of effective protecting coatings has not been defined yet, values of pore resistance (R_p) at least equal to 10^6–10^7 Ω cm^2 can be found in the literature [53,61]. In the present work, we decided to empirically set an even higher threshold equal to 10^9 Ω cm^2 [59]. While at the beginning of the test, all the cured coatings neatly overcome the set threshold, already at the end of the ca.1-day natural aging sample PC_2:1_3 does not completely satisfy the reference value. After the threshold of six cycles, according to ISO 17463, EIS reveals good preservation of the protection performance for all the remaining coatings, with pore resistance higher than 1 GΩ cm^2 (Fig. 9). On the contrary, sample PC_2:1_3 exhibits a further but slight decrease of resistance, reaching a value around 0.2 GΩ cm^2.

For all tested coatings, the film capacitance is around 100 pF cm^{-2} with a relative water uptake below 6 % (Fig. 9), both evaluated at the end of the 6-cycle ACET run. No significant variation was detected when compared to the values at the end of the natural aging step. Interestingly, the growth rate of all figures of merit is significantly smoothed than that recorded for the first 24 h of immersion at open circuit conditions, evidencing good robustness of the coatings to the accelerated aging (Figure S8). This is even more relevant considering that samples were subjected to a more extreme cathodic polarization than the minimum one suggested by the standard ISO procedure (i.e., –4 V vs AgCl/Ag with respect to –2V), which means a higher electric field for the migration of solvated ions and higher energy for triggering the electroreduction reaction.

The accelerated aging process was exacerbated by reaching a seven-time longer aging period (42 cycles, lasting 7 days) before evaluating the final protection performance of the novel bio-based corrosion protective coatings (Fig. 9 and Figure S9). During this extra period, the control parameters reached soon almost stationary values or showed a slight reduction over time. In any case, no abrupt changes were detected, thus excluding the occurrence of one or more critical sudden deterioration processes of the coatings even during a 7 times longer accelerated aging period (Figure S8). The relative ranking among novel coatings did not change even after one week of accelerated test, with PC_5:1_3 and PC_4:1_5 being the most performing bio-based formulations with R_p around 1 GΩ cm^2 (Fig. 9).

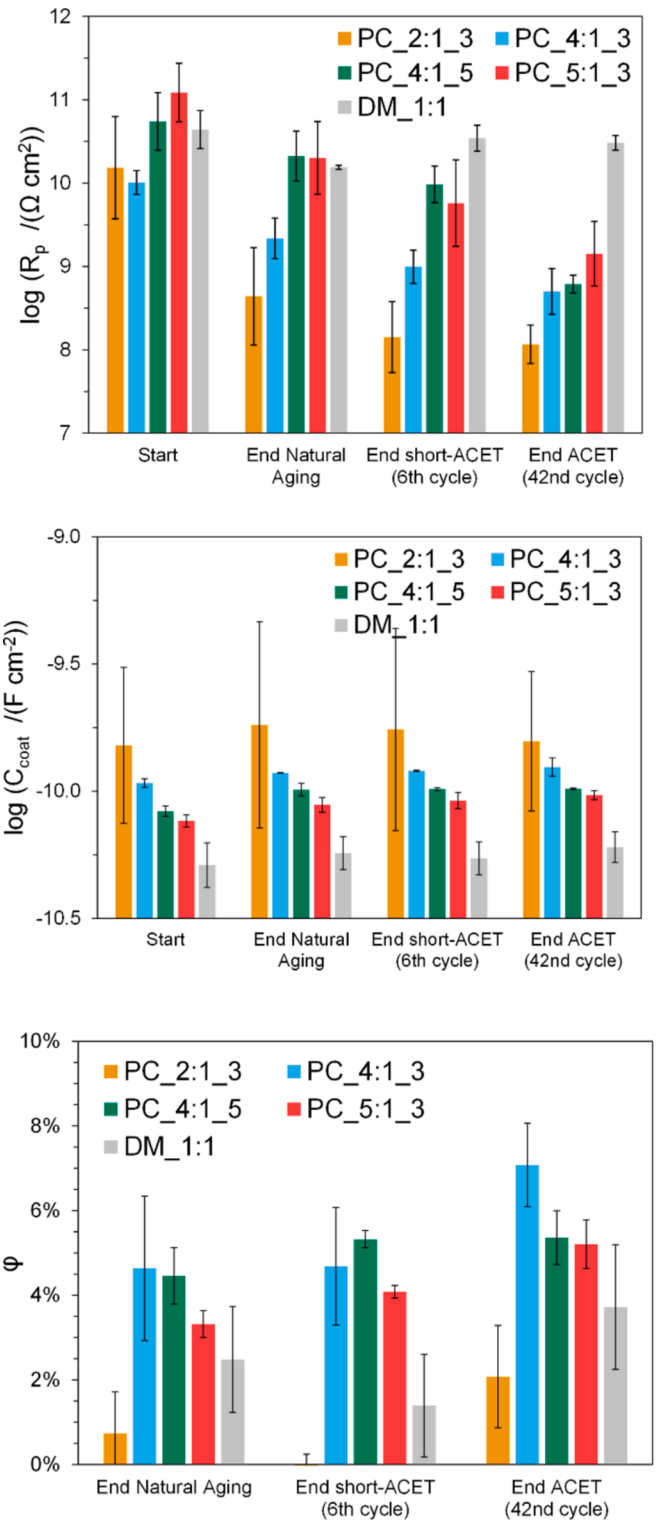

Fig. 9. Comparison of the figure of merits for coated samples at representative times: starting, end of natural aging period, end of classical ACET (6 cycles), end of long ACET (42 cycles).

4. Conclusions

In this work, 10,16-diHHDA was obtained with an average purity of 92 wt% and a recovery efficiency of 67 %, higher than those reported in the literature. Moreover, this study presents the first demonstration of epoxy resins successfully cured with the highly pure cutin monomer. A fine-tuning of bio-based epoxy coating formulations was performed by

introducing a required amount of curing agent over epoxy reactive units of the precursors. For the phloroglucinol epoxy coatings series, an increase in the molar epoxy/X–H ratio (up to 5:1) resulted in higher T_g values, corresponding to a higher conversion of crosslinking reaction. A higher percentage of catalyst (i.e., 5 mol%) was also found beneficial in raising the T_g to an average of 104 °C. The increase in crosslinking conversion and T_g resulted in a noticeable improvement in the coating's hardness and adhesion strength. The latter properties are probably due to a higher content of stiff and aromatic segments in the coatings, strengthening the interactions with metallic substrates.

Subjected to a long-lasting accelerated electrochemical aging test, phloroglucinol-based resins with a molar epoxy/X–H ratio of 4 and 5 and with a 5 % and 3 % mol. catalyst concentration, respectively, (i.e. PC_5:1_3 and PC_4:1_5) showed excellent performance in terms of water barrier and corrosion protection, by neatly outperforming similar bio-based coatings reported in the literature. The formulations demonstrated high pore resistance ($\geq$1 GΩ cm^2), low capacitance (<100 pF cm^{-2}), and low volumetric water uptake (<5 %). In similar stress conditions, the petrol-based benchmark exhibited a pore resistance one order of magnitude higher, suggesting a slower deterioration over time. However, there was no significant difference in relative water uptake for the best-performing cutin-derived coatings, especially extrapolating the future trend by the almost linear behavior detected during the long-lasting ACET aging test.

All these findings demonstrate that the cutin monomer 10,16-diHHDA can be successfully crosslinked with other resins, excluding the curing to be affected by any synergistic effects by compounds invariably co-present in the mixtures previously reported in analogous literature studies. Along with our previous papers, this work therefore highlights the potential of tomato peels as a secondary source of dihydro aliphatic carboxylic acid, acting as a versatile curing agent for bio-based organic coatings. Also, the newly developed bio-derived coatings are a good alternative to commercially available petrol-based counterparts, especially those containing harmful bisphenol A.

Funding Sources

This research was funded by Fondazione Cariplo in the framework of the 2021 Call "Circular economy for a sustainable future, for the project entitled "Cutin from Tomato-peel waste: green source for plurality of engineered polymer Products (CutToPro)", grant number: 2021-0651. The research activities of M.M. are supported by the Italian Ministry of Education, University and Research (MIUR) and European Social Fund (ESF) through the PON 2014-2020 program, action IV.6 'Research contracts on green issues'.

Declaration of generative AI and AI-assisted technologies in the writing process

During the preparation of this work, the authors used the tool Grammarly to improve the readability and language of the manuscript. After using this tool, the authors reviewed and edited the content as needed and took full responsibility for the content of the published article.

CRediT authorship contribution statement

Raffaella Suriano: Writing – review & editing, Writing – original draft, Supervision, Project administration, Funding acquisition, Conceptualization. **Mirko Magni:** Writing – review & editing, Writing – original draft, Supervision, Methodology, Conceptualization. **Beatrice Tagliabue:** Visualization, Validation, Investigation, Data curation. **Valentina Re:** Investigation, Data curation. **Riccardo Ciapponi:** Investigation, Data curation. **Rita Nasti:** Writing – review & editing, Methodology, Investigation. **Marco Cavallaro:** Writing – review & editing. **Giangiacomo Beretta:** Resources, Project administration, Funding acquisition. **Stefano Turri:** Writing – review & editing, Resources, Funding acquisition. **Marinella Levi:** Resources.

Declaration of competing interest

The authors declare that they have no known competing financial interests or personal relationships that could have appeared to influence the work reported in this paper.

Acknowledgment

Besides thanking the funding sources listed in the dedicated section, the authors also thank Tomato Farm S.p.A for kindly providing tomato pomace and Nagase ChemteX Co. for kindly supplying the sorbitol-based resins. M.M. thanks Engitec Technologies for co-funding his research period 2022-2024. The authors deeply thank Alireza Safdari for his contribution in the creation of the graphical abstract.

Appendix A. Supplementary material

Supplementary data to this article can be found online at https://doi.org/10.1016/j.eurpolymj.2024.113629.

Data availability

Data will be made available on request.

References

[1] C. Ingrao, J. Bacenetti, A. Bezama, V. Blok, P. Goglio, E.G. Koukios, M. Lindner, T. Nemecek, V. Siracusa, A. Zabaniotou, D. Huisingh, The potential roles of bio-economy in the transition to equitable, sustainable, post fossil-carbon societies: findings from this virtual special issue, J. Clean. Prod. 204 (2018) 471–488, https://doi.org/10.1016/j.jclepro.2018.09.068.

[2] EC bioeconomy webpage. https://research-and-innovation.ec.europa.eu/research-area/environment/bioeconomy_en#:~:text=The%20bioeconomy%20means%20using%20renewable,circular%20and%20low%2Dcarbon%20economy. (accessed July 2023).

[3] P.R. Yaashikaa, P. Senthil Kumar, S. Varjani, Valorization of agro-industrial wastes for biorefinery process and circular bioeconomy: A critical review, Bioresour. Technol. 343 (2022) 126126, https://doi.org/10.1016/j.biortech.2021.126126.

[4] F. Haque, C. Fan, Y.-Y. Lee, From waste to value: Addressing the relevance of waste recovery to agricultural sector in line with circular economy, J. Clean. Prod. 415 (2023) 137873, https://doi.org/10.1016/j.jclepro.2023.137873.

[5] F. Boccia, P. Di Donato, D. Covino, A. Poli, Food waste and bio-economy: A scenario for the Italian tomato market, J. Clean. Prod. 227 (2019) 424–433, https://doi.org/10.1016/j.jclepro.2019.04.180.

[6] L. Xue, Z. Cao, S. Scherhaufer, K. Östergren, S. Cheng, G. Liu, Mapping the EU tomato supply chain from farm to fork for greenhouse gas emission mitigation strategies, J. Ind. Ecol. 25 (2021) 377–389, https://doi.org/10.1111/jiec.13080.

[7] EU statistics on tomatoes production, prices and trade. https://agriculture.ec.europa.eu/data-and-analysis/markets/overviews/market-observatories/fruit-and-vegetables/tomatoes-statistics_en (accessed July 2023).

[8] M.J. Fernández-Gómez, M. Díaz-Raviña, E. Romero, R. Nogales, Recycling of environmentally problematic plant wastes generated from greenhouse tomato crops through vermicomposting, Int. J. Environ. Sci. Technol. 10 (2013) 697–708, https://doi.org/10.1007/s13762-013-0239-7.

[9] A. Scoma, S. Rebecchi, L. Bertin, F. Fava, High impact biowastes from South European agro-industries as feedstock for second-generation biorefineries, Crit. Rev. Biotechnol. 36 (2016) 175–189, https://doi.org/10.3109/07388551.2014.947238.

[10] A.N. Grassino, J. Halambek, S. Djaković, S. Rimac Brnčić, M. Dent, Z. Grabarić, Utilization of tomato peel waste from canning factory as a potential source for pectin production and application as tin corrosion inhibitor, Food Hydrocoll. 52 (2016) 265–274, https://doi.org/10.1016/j.foodhyd.2015.06.020.

[11] J.A. Heredia-Guerrero, A. Heredia, E. Domínguez, R. Cingolani, I.S. Bayer, A. Athanassiou, J.J. Benítez, Cutin from agro-waste as a raw material for the production of bioplastics, J. Exp. Bot. 68 (2017) 5401–5410, https://doi.org/10.1093/jxb/erx272.

[12] G.I.C. Righetti, R. Nasti, G. Beretta, M. Levi, S. Turri, R. Suriano, Unveiling the hidden properties of tomato peels: cutin ester derivatives as bio-based plasticizers for polylactic acid, Polymers 15 (2023) 1848, https://doi.org/10.3390/polym15081848.

[13] A. Heredia, Biophysical and biochemical characteristics of cutin, a plant barrier biopolymer, Biochim. Biophys. Acta - Gen. Subj. 1620 (2003) 1–7, https://doi.org/10.1016/S0304-4165(02)00510-X.

[14] D. Arrieta-Baez, M. Cruz-Carrillo, M.B. Gómez-Patiño, L.G. Zepeda-Vallejo, Derivatives of 10,16-dihydroxyhexadecanoic acid isolated from tomato (solanum lycopersicum) as potential material for aliphatic polyesters, Molecules 16 (2011) 4923–4936, https://doi.org/10.3390/molecules16064923.
[15] J.J. Benítez, P.M. Castillo, J.C. Del Río, M. León-Camacho, E. Domínguez, A. Heredia, S. Guzmán-Puyol, A. Athanassiou, J.A. Heredia-Guerrero, Valorization of tomato processing by-products: fatty acid extraction and production of bio-based materials, Materials 11 (2018) 2211, https://doi.org/10.3390/ma11112211.
[16] E. Ruffini, A. Bianchi Oltolini, M. Magni, G. Beretta, M. Cavallaro, R. Suriano, S. Turri, Crosslinked polyesters as fully biobased coatings with cutin monomer from tomato peel wastes, Polymers 16 (2024) 682, https://doi.org/10.3390/polym16050682.
[17] J.J. Benítez, S. Osbild, S. Guzman-Puyol, A. Heredia, J.A. Heredia-Guerrero, Bio-based coatings for food metal packaging inspired in biopolyester plant cutin, Polymers 12 (2020) 942, https://doi.org/10.3390/polym12040942.
[18] A. Montanari, L. Bolzoni, I.M. Cigognini, A. Ciruelos, M. Gòmez Cardoso, R. de la Torre In *Tomato bio-based lacquer for sustainable metal packaging*, XIV International Symposium on Processing Tomato, Leuven, Belgium, ISHS Acta Horticulturae: Leuven, Belgium, 2017; pp 159-166, doi: 10.17660/ActaHortic.2017.1159.24.
[19] J.J. Benítez, M.C. Ramírez-Pozo, M.M. Durán-Barrantes, A. Heredia, G. Tedeschi, L. Ceseracciu, S. Guzman-Puyol, D. Marrero-López, A. Becci, A. Amato, J. A. Heredia-Guerrero, Bio-based lacquers from industrially processed tomato pomace for sustainable metal food packaging, J. Clean. Prod. 386 (2023) 135836, https://doi.org/10.1016/j.jclepro.2022.135836.
[20] J.A. Heredia-Guerrero, C.A. Williams, G. Guidetti, P. Cataldi, L. Ceseracciu, D. Debellis, A. Athanassiou, S. Guzman-Puyol, W.Y. Hamad, S. Vignolini, Plant-inspired polyaleuritate–nanocellulose composite photonic films, ACS Appl. Polym. Mater. 2 (2020) 1528–1534, https://doi.org/10.1021/acsapm.9b01205.
[21] J.J. Benítez, J.A. Heredia-Guerrero, S. Guzmán-Puyol, E. Domínguez, A. Heredia, Long-chain polyhydroxyesters from natural occurring aleuritic acid as potential material for food packaging, Soft Mater. 13 (2015) 5–11, https://doi.org/10.1080/1539445X.2014.993476.
[22] E. Buratti, D. Scittarelli, L.A. Lerin, A. Odoardo, A. D'Iorio, M. Calosi, F. Petri, A. Montanari, A. Balbo, M. Bertoldo, Development of biobased poly(ester-urethane) coatings with excellent hydrophobicity from tomato byproducts, ACS Sustain. Chem. Eng. 12 (2024) 6856–6869, https://doi.org/10.1021/acssuschemeng.3c06052.
[23] C. Flosbach, R. Fugier, Epoxy Functional Acrylic Polymers for High Performance Coating Applications, in: J.-.-P. Pascault, R.J.J. Williams (Eds.), Epoxy Polymers, John Wiley & Sons, 2010, pp. 39–54.
[24] H.Q. Pham, M.J. Marks, Epoxy Resins. Ullmann's Encyclopedia of Industrial Chemistry, Wiley-VCH, 2012.
[25] L. Pierau, C. Elian, J. Akimoto, Y. Ito, S. Caillol, D.-L. Versace, Bio-sourced monomers and cationic photopolymerization–The green combination towards eco-friendly and non-toxic materials, Prog. Polym. Sci. 127 (2022) 101517, https://doi.org/10.1016/j.progpolymsci.2022.101517.
[26] H. Okada, T. Tokunaga, X. Liu, S. Takayanagi, A. Matsushima, Y. Shimohigashi, Direct evidence revealing structural elements essential for the high binding ability of bisphenol a to human estrogen-related receptor-γ, Environ. Health Perspect. 116 (2008) 32–38, https://doi.org/10.1289/ehp.10587.
[27] H. Sreehari, A.S. Sethulekshmi, A. Saritha, Bio epoxy coatings: an emergent green anticorrosive coating for the future, Macromol. Mater. Eng. 307 (2022) 2200004, https://doi.org/10.1002/mame.202200004.
[28] D.A. Bellido-Aguilar, S. Zheng, Y. Huang, Y. Sun, X. Zeng, Q. Zhang, Z. Chen, Hydrophobization of fully bio-based epoxy polymers using water as solvent: effect of additives, Eur. Polym. J. 140 (2020) 110043, https://doi.org/10.1016/j.eurpolymj.2020.110043.
[29] D.A. Bellido-Aguilar, S. Zheng, Y. Huang, X. Zeng, Q. Zhang, Z. Chen, Solvent-free synthesis and hydrophobization of biobased epoxy coatings for anti-icing and anticorrosion applications, ACS Sustain. Chem. Eng. 7 (2019) 19131–19141, https://doi.org/10.1021/acssuschemeng.9b05091.
[30] L.R.R. da Silva, F. Avelino, O.B.F. Diogenes, V.d.O.F. Sales, K.T. da Silva, W. S. Araujo, S.E. Mazzetto, D. Lomonaco, Development of BPA-free anticorrosive epoxy coatings from agroindustrial waste, Prog. Org. Coat. 139 (2020) 105449, https://doi.org/10.1016/j.porgcoat.2019.105449.
[31] P. Singh, A. Rana, N. Karak, I. Kumar, S. Rana, P. Kumar, Sustainable smart anti-corrosion coating materials derived from vegetable oil derivatives: a review, RSC Adv. 13 (2023) 3910–3941, https://doi.org/10.1039/D2RA07825B.
[32] J. Pouladi, S.M. Mirabedini, H. Eivaz Mohammadloo, N.G. Rad, Synthesis of novel plant oil-based isocyanate-free urethane coatings and study of their anti-corrosion properties, Eur. Polym. J. 153 (2021) 110502, https://doi.org/10.1016/j.eurpolymj.2021.110502.
[33] S. Zheng, D.A. Bellido-Aguilar, Y. Huang, X. Zeng, Q. Zhang, Z. Chen, Mechanically robust hydrophobic bio-based epoxy coatings for anti-corrosion application, Surf. Coat. Technol. 363 (2019) 43–50, https://doi.org/10.1016/j.surfcoat.2019.02.020.
[34] N. Lorwanishpaisarn, N. Srikhao, K. Jetsrisuparb, J.T.N. Knijnenburg, S. Theerakulpisut, M. Okhawilai, P. Kasemsiri, Self-healing ability of epoxy vitrimer nanocomposites containing bio-based curing agents and carbon nanotubes for corrosion protection, J. Polym. Environ. 30 (2022) 472–482, https://doi.org/10.1007/s10924-021-02213-3.
[35] N. Lorwanishpaisarn, P. Kasemsiri, N. Srikhao, K. Jetsrisuparb, J.T.N. Knijnenburg, S. Hiziroglu, U. Pongsa, P. Chindaprasirt, Fabrication of durable superhydrophobic epoxy/cashew nut shell liquid based coating containing flower-like zinc oxide for continuous oil/water separation, Surf. Coat. Technol. 366 (2019) 106–113, https://doi.org/10.1016/j.surfcoat.2019.03.021.
[36] C. Lu, Y. Liu, C. Wang, Q. Yong, J. Wang, F. Chu, An integrated strategy to fabricate bio-based dual-cure and toughened epoxy thermosets with photothermal conversion property, Chem. Eng. J. 433 (2022) 134582, https://doi.org/10.1016/j.cej.2022.134582.
[37] S.F. Osman, P. Irwin, W.F. Fett, J.V. O'Conno, N. Parris, Preparation, isolation, and characterization of cutin monomers and oligomers from tomato peels, J. Agric. Food Chem. 47 (1999) 799–802, https://doi.org/10.1021/jf980693r.
[38] D.K. Owens, R.C. Wendt, Estimation of the surface free energy of polymers, J. Appl. Polym. Sci. 13 (1969) 1741–1747, https://doi.org/10.1002/app.1969.070130815.
[39] I.N. Sneddon, The relation between load and penetration in the axisymmetric boussinesq problem for a punch of arbitrary profile, Int. J. Eng. Sci. 3 (1965) 47–57, https://doi.org/10.1016/0020-7225(65)90019-4.
[40] S. Saseendran, M. Wysocki, J. Varna, Cure-state dependent viscoelastic Poisson's ratio of LY5052 epoxy resin, Adv. Manuf.: Polym. Compos. Sci. 3 (2017) 92–100, https://doi.org/10.1080/20550340.2017.1348002.
[41] V. Sundararaghavan, A. Kumar, Molecular dynamics simulations of compressive yielding in cross-linked epoxies in the context of Argon theory, Int. J. Plast. 47 (2013) 111–125, https://doi.org/10.1016/j.ijplas.2013.01.004.
[42] R. Suriano, C. Credi, M. Levi, S. Turri, AFM nanoscale indentation in air of polymeric and hybrid materials with highly different stiffness, Appl. Surf. Sci. 311 (2014) 558–566, https://doi.org/10.1016/j.apsusc.2014.05.108.
[43] International Organization for Standardization. Paints and varnishes. Determination of film hardness by pencil test, 2020.
[44] ISO 4624:2016, Paints and varnishes — Pull-off test for adhesion, 2016.
[45] ISO, ISO17463, Paints and varnishes - Guidelines for the determination of anticorrosive properties of organic coatings by accelerated cyclic electrochemical technique, 2022.
[46] A. Demongeot, R. Groote, H. Goossens, T. Hoeks, F. Tournilhac, L. Leibler, Cross-linking of poly(butylene terephthalate) by reactive extrusion using Zn(II) epoxy-vitrimer chemistry, Macromolecules 50 (2017) 6117–6127, https://doi.org/10.1021/acs.macromol.7b01141.
[47] G. Socrates, Infrared and Raman characteristic group frequencies: tables and charts, 3rd ed., John Wiley & Sons Ltd, Chichester, 2001.
[48] Y.R. Ham, S.H. Kim, Y.J. Shin, D.H. Lee, M. Yang, J.H. Min, J.S. Shin, A comparison of some imidazoles in the curing of epoxy resin, J. Ind. Eng. Chem. 16 (2010) 556–559, https://doi.org/10.1016/j.jiec.2010.03.022.
[49] F. Ng, L. Bonnet, G. David, S. Caillol, Novel biobased and food contact epoxy coatings for glass toughening applications, Prog. Org. Coat. 109 (2017) 1–8, https://doi.org/10.1016/j.porgcoat.2017.04.008.
[50] D. Guzmán, D. Santiago, À. Serra, F. Ferrando, Novel bio-based epoxy thermosets based on triglycidyl phloroglucinol prepared by thiol-epoxy reaction, Polymers 12 (2020) 337, https://doi.org/10.3390/polym12020337.
[51] A. Bahrami, X. Morelle, L.D. Hông Minh, T. Pardoen, C. Bailly, B. Nysten, Curing dependent spatial heterogeneity of mechanical response in epoxy resins revealed by atomic force microscopy, Polymer 68 (2015) 1–10, https://doi.org/10.1016/j.polymer.2015.04.084.
[52] D. Haba, J. Kaufmann, A.J. Brunner, K. Resch, C. Teichert, Observation of elastic modulus inhomogeneities in thermosetting epoxies using AFM – Discerning facts and artifacts, Polymer 55 (2014) 4032–4040, https://doi.org/10.1016/j.polymer.2014.06.030.
[53] A. Amirudin, D. Thieny, Application of electrochemical impedance spectroscopy to study the degradation of polymer-coated metals, Prog. Org. Coat. 26 (1995) 1–28, https://doi.org/10.1016/0300-9440(95)00581-1.
[54] A. Trentin, A. Pakseresht, A. Duran, Y. Castro, D. Galusek, Electrochemical characterization of polymeric coatings for corrosion protection: a review of advances and perspectives, Polymers 14 (2022) 2306, https://doi.org/10.3390/polym14122306.
[55] G. Grundmeier, W. Schmidt, M. Stratmann, Corrosion protection by organic coatings: electrochemical mechanism and novel methods of investigation, Electrochim. Acta 45 (2000) 2515–2533, https://doi.org/10.1016/S0013-4686(00)00348-0.
[56] G.J. Brug, A.L.G. van den Eeden, M. Sluyters-Rehbach, J.H. Sluyters, The analysis of electrode impedances complicated by the presence of a constant phase element, J. Electroanal. Chem. Interf. Electrochem. 176 (1984) 275–295, https://doi.org/10.1016/S0022-0728(84)80324-1.
[57] J. Hollaender, Rapid assessment of food/package interactions by electrochemical impedance spectroscopy (EIS), Food Addit. Contam. 14 (1997) 617–626, https://doi.org/10.1080/02652039709374574.
[58] M.J. Gimeno, S. Chamorro, R. March, E. Oró, P. Pérez, J. Gracenea, J. Suay, Anticorrosive properties enhancement by means of phosphate pigments in an epoxy 2k coating. Assessment by NSS and ACET, Prog. Org. Coat. 77 (2014) 2024–2030, https://doi.org/10.1016/j.porgcoat.2014.04.004.
[59] ISO 17463:2022 Paints and varnishes— Guidelines for the determination of anticorrosive properties of organic coatings by accelerated cyclic electrochemical technique. , 2022.
[60] S.I. Bhat, M. Mobin, S. Islam, S. Zehra, I., Shahid ul, Recent advances in anticorrosive coatings based on sustainable polymers: challenges and perspectives, Surf. Coat. Technol. 480 (2024) 130596, https://doi.org/10.1016/j.surfcoat.2024.130596.
[61] M. Salzano de Luna, Recent trends in waterborne and bio-based polyurethane coatings for corrosion protection, Adv. Mater. Interf. 9 (2022) 2101775, https://doi.org/10.1002/admi.202101775.